Application of SHS in the Manufacture of (NiAl/Ni_3Al)/TiB_2 Composite

P. HYJEK, I. SULIMA, and L. JAWORSKA

The aim of this study was to demonstrate the advantages and the method of application of the SHS process in the manufacture of (NiAl/Ni_3Al)/TiB_2 composites. A comparison was made between sinters manufactured by FAST/SPS using two different routes to process the substrates, which formed the composite matrix. The evaluation criteria were based on measurements of selected physical, mechanical, and tribological properties, and on microstructure examinations. The evaluation has indicated a preferable method for the manufacture of composites, where the SHS reaction takes place during compaction of the powder mixture. This produces a sinter characterized not only by the high degree of sintering, and high values of the Young's modulus and HV1 hardness, but also by the satisfactory resistance to tribological wear. Additionally, the use of this process saves energy and reduces product-making cost, owing to a less expensive technique of making individual substrates.

https://doi.org/10.1007/s11661-019-05306-w

I. INTRODUCTION

ALLOYS based on NiAl phases are perceived as interesting materials for applications in the energy, manufacturing, automotive, and aerospace industries. This is related to their potentially high operating temperature, as they are characterized by high thermal stability, including good mechanical properties at high temperature, relatively low density, satisfactory corrosion resistance, and resistance to oxidation.[1–4]

The high-temperature mechanical properties can be further improved when NiAl-based composites with evenly spaced, very hard ceramic particles are produced, *e.g.*, TiB_2, ZrB_2, Al_2O_3, CeO_2, ZrO_2, or TiC.[5–12] It has been found that the reinforcing particles significantly improve the NiAl compressive strength at both room and high temperature (up to 1100 °C].[12,13] Such composites are also characterized by good resistance to erosive wear and corrosion, especially at high operating temperatures.[9,14–16] Borides, mainly ZrB_2 and TiB_2, are particularly suitable for this application, due to their inertness to NiAl.[17,18]

Intermetallic materials, although usually capable of offering satisfactory mechanical properties at high temperature, seem to be very brittle at room temperature. Reducing the grain size can solve to some extent this problem and extend the range of their practical use. Therefore, powder metallurgy is a technological alternative in the manufacture of NiAl alloys and composites based on the NiAl intermetallic matrix with a sufficiently high dispersion of the reinforcing phase.[19,20]

This study focuses on the self-propagating high-temperature synthesis (SHS) of composites based on the NiAl intermetallic matrix (IMCs).

SHS is an effective and cheap method to produce various materials useful in the industry. Extensive studies conducted in this field underline numerous favorable aspects of this method when applied in the manufacture of materials, including energy savings and environmental protection. SHS has become an important technique for the synthesis and processing of composites, alloys, intermetallic compounds, nanomaterials, and advanced ceramics, both structural and functional.[21–25] Processes of combustion synthesis are characterized by high values of temperature, fast heating rates, and short reaction time. This makes SHS an attractive tool in the production of materials, due to the lower manufacturing cost compared to traditional processes. Other advantages of SHS include the use of relatively simple equipment, making high purity products in practically any size and shape, stabilization of metastable phases, fine grain sizes and strong bonds formed between substantially different phases (ceramic and metallic).[26,27]

P. HYJEK and I. SULIMA are with the Pedagogical University of Cracow, Institute of Technology, Kraków, Poland. Contact e-mail: pawel.hyjek@up.krakow.pl L. JAWORSKA is with the AGH University of Science and Technology, Faculty of Non-Ferrous Metals, Al. A. Mickiewicza 30, 30-059 Kraków, Poland.

Manuscript submitted September 20, 2018.
Article published online June 3, 2019

The SHS method is based on the use of heat generated by the energy of exothermic reactions occurring between substrates during the process of synthesis to preheat the system to the required temperature and maintain this temperature until the reactants are fully converted into reaction products.[28] Often materials produced by SHS are characterized by high porosity,[29,30] but this can be avoided by simultaneous synthesis and consolidation of material in the sintering process. This route of the NiAl alloy and NiAl-Al_2O_3 composite manufacture using pulse plasma sintering (PPS) and SHS reaction was adopted by Reference 31, and positive results were obtained in the form of high relative density, hardness, and fracture toughness.

Compared to porous 316L (316LSS) stainless steel, the porous NiAl provides better resistance to oxidation under given conditions, which can be a promising alternative in hard working environments.[32]

One of the recently developed methods ensuring very effective powder consolidation with pulsating electric current is spark plasma sintering (SPS). Compared to conventional hot pressing, the use of this innovative technique seems to offer many additional advantages, and while the hot pressing (HP) technology demands relatively long production times (in the order of hours), sintering by SPS is a very rapid process (several minutes), since the electric current passing through the feedstock significantly raises the heating speed due to the Joule effect. Another important factor is the availability of many different routes for the synthesis of powders by SPS, thus enabling a more effective consolidation, particularly important in the case of hard-to-sinter heat-resistant ceramic materials.[33–35]

Various mechanisms and phenomena were described to emphasize numerous benefits derived from the use of SPS.[36] It has been demonstrated that the same benefits are also obtained when the reactions of synthesis and densification are accomplished in one step by means of the, so-called, reactive SPS (R/SPS). Considering the above, high-density advanced materials with uniform and fine microstructure can be produced in a relatively short time.

Another method to produce fine-grained materials based on the NiAl intermetallic matrix is the two-step process described in Reference 37. In the first stage, an intermetallic alloy is made by the SHS process. This alloy is next ground to a very fine powder and sintered, preferably in a sufficiently short time to avoid grain growth. Studies using two methods to produce ultra-high-temperature ceramics (UHTC) by SPS were carried out by Reference 38. In the first method, ceramic powders were first synthesized by SHS, and then sintered by SPS. In the second method, called reactive SPS (R/SPS), the material was synthesized and compacted in one step. Based on the results obtained in the above-mentioned tests, analogical tests and studies were conducted using as a test material the NiAl-based composite. The results and conclusions are presented in the article. The designations of the sinters produced (Table I) were the same as in Orrù and Cao,[38] consistent with the adopted fabrication procedure.

Composites based on single-phase and two-phase nickel-aluminum matrix have already been produced by casting in a Balzers type furnace, HPHT sintering in a Bridgman type chamber, and FAST/SPS synthesis. Positive results obtained for composites based on a two-phase NiAl/Ni_3Al matrix with the addition of 3 wt pct TiB_2 encouraged the authors of this article to carry out further research in this area. Previous studies[39] of the manufacture of these composites allowed selecting optimal conditions for the FAST/SPS process. The composite matrix was a two-phase NiAl/Ni_3Al alloy fabricated from commercial Ni79Al21 powder. According to the manufacturer, it was produced by sintering a mixture of powders of constituent metals. The resulting cake was ground and sieved to the required particle size. During sintering, an exothermic reaction (SHS) occurred and the obtained product was characterized by a two-phase structure.

The identification of efficient manufacturing techniques is very important considering their rapid and large-scale development. Accordingly, this article describes the use of SHS in combination with FAST/SPS to obtain a fine grain (NiAl/Ni_3Al)/TiB_2 composite characterized by a very high degree of compaction.

II. EXPERIMENTAL

Two FAST/SPS routes and powder grains of similar size and shape were used to produce the NiAl/Ni_3Al + 3 wt pct TiB_2 composite. The same pressure-current parameters were applied. The list of individual powders with their characteristics and designations is presented in Table I. The morphology of powder grains used in the manufacture of SPS composite is described in more detail in Reference 40. The commercial NiAl powder (Ni79Al21 wt pct) was composed of flaky grains of the size smaller than the minimum size specified by the manufacturer (45 μm) with sporadically occurring large grains of a globular shape (approx. 100 μm in size). Grains with the maximum size specified by the manufacturer were not found.

To produce R/SPS composites from the technically pure elementary powders of nickel, aluminum, and titanium diboride, appropriate mixtures were prepared—(79 pct Ni + 21 pct Al) + 3 pct TiB_2 (wt pct).

Observations and SEM examinations showed the grain size of nickel powder different than that specified by the manufacturer (estimated on the basis of sieve analysis). As a result, one could have the impression that nickel powder was composed of the grains with a maximum size of 10 μm. Aluminum powder contained both small grains of the size close to 1 μm and larger grains of the size approaching 100 μm, and this was consistent with the manufacturer's specification—10 pct of grains are below 5 to 15 μm, 50 pct of grains are below 20 to 35 μm, 90 pct of grains are below 50 to 85 μm.

The morphology of grains in the Ni + Al + TiB_2 mixture prepared by the procedure described below is shown in Figure 1. The sintering parameters and the

Table I. The Sintering Parameters and the Characteristics of Individual Powders

Sinter Type	Powder (Wt Pct)	Grain Parameters		Production Procedure
		Size (μm)	Purity (Pct)	
Composite SPS	Ni79Al21	< 150	99.0	sintering by SHS, grinding, mixing, sintering
	3 pct TiB_2	2.5 to 3.5	99.9	by FAST/SPS (T = 1150 °C, P = 48 MPa, t = 10 min)
Composite R/SPS	(79 pct Ni	< 150	99.99	mixing, sintering by FAST/SPS (T = 1000 °C,
	21 pct Al)	< 100	99.7	P = 48 MPa, t = 0.5 min)
	3 pct TiB_2	2.5 to 3.5	99.9	

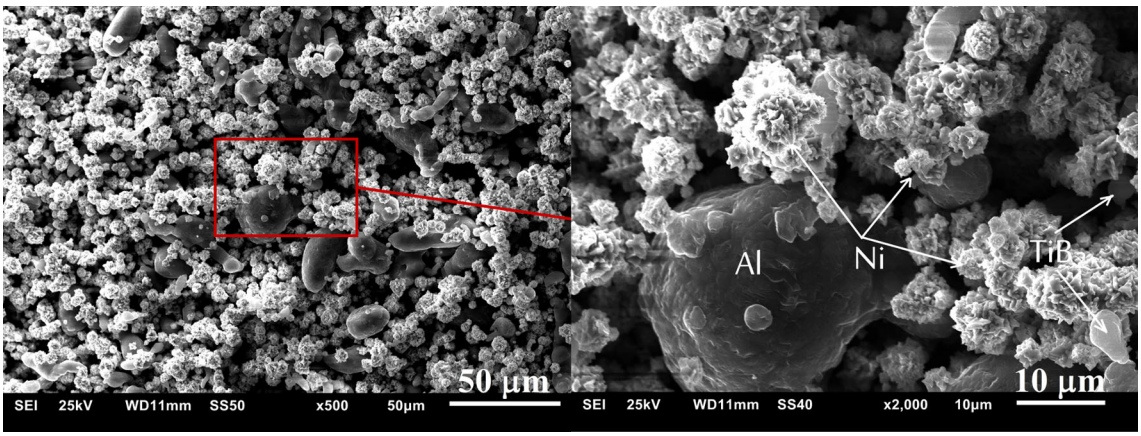

Fig. 1—Mixture of Ni + Al + TiB_2 powders used in the process of making R/SPS composite shown in two different magnifications.

characteristics of individual powders are included in Table I.

For both types of composites, mixing of powders with the grinding media, which were steel balls in a 10:1 weight ratio, was carried out for 20 hours in a Turbula device until a uniform distribution of the ceramic particles was obtained. Then, the powder feedstock was sintered by FAST/SPS in an argon atmosphere under a pressure of 48 MPa at a constant heating rate of 85 °C/min. For the SPS composite, the sintering time and temperature were 10 minutes and 1150 °C, respectively. In the case of the R/SPS composite, a lower temperature of 1000 °C and a shorter time of 0.5 minute were applied to obtain a similar high-quality end product characterized by the high degree of sintering and low porosity. The parameters were determined from the graph showing process run in real time, plotted until the piston movement stopped, thus indicating almost full compaction of powder (Figure 2).

Sinters with a diameter of 20 mm and a height of 5 mm were produced in an FCT HP5 device.

After cleaning and surface preparation, the density and porosity were measured by the hydrostatic method, while Young's modulus was determined by ultrasounds using Panametrics Epoch III ultrasonic flaw detector. The HV1 hardness and HV0.05 microhardness were determined with a NEXUS 4000 hardness tester. Phase identification was carried out by X-ray diffraction using Cu Kα radiation. General condition of the sintered compact was evaluated by examinations of its microstructure using for this purpose an Olympus GX-51 optical microscope and a JEOL JSM 6460 LV scanning microscope. The abrasion resistance of produced materials was tested in accordance with ASTM G99-05. In ball-on-disc tests, an ELBIT universal tester for tribological tests was used. The following test parameters were applied: Load F = 5 N, Radius of the wear track R—6 mm, Ball diameter r—1/8'', Al_2O_3, Velocity V= 0.12 m/s, Test duration t = 10,000 seconds, Environment-Air, Chamber Temperature T_c = 25 °C, Chamber Humidity H_c = 20.5 pct.

The coefficient of friction and furrow size (scar depth) were automatically measured and recorded for each test. The scar depth allowed determining the linear wear intensity.

III. RESULTS AND DISCUSSION

A. *Record of the Process Run*

When the mixture of Ni, Al, and TiB_2 powders is sintered (R/SPS composite) and the temperature rises to about 575 °C, an exothermic reaction starts. Owing to one of the advantages of the device used, which is the possibility of real-time observation of the process run and changes in its parameters, significant differences

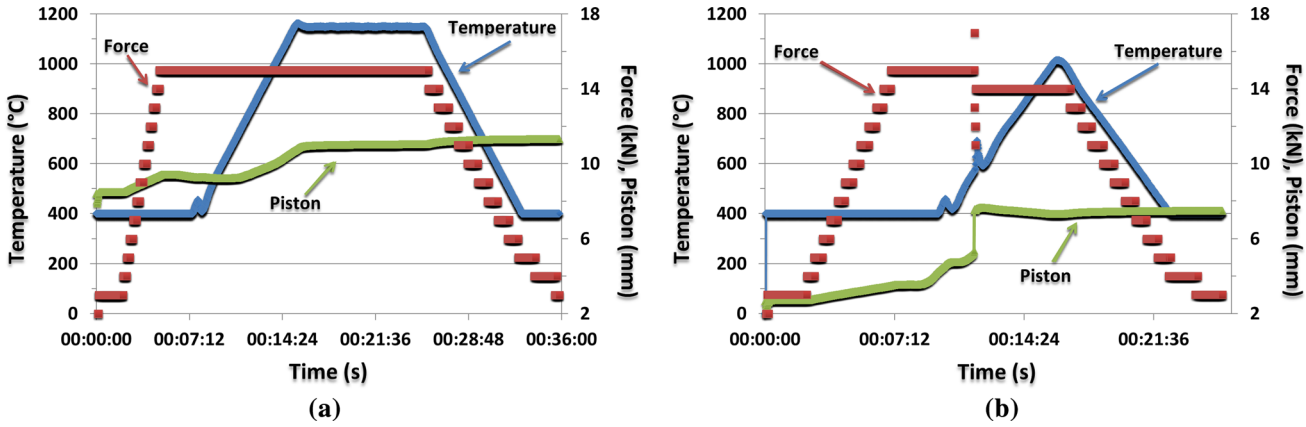

Fig. 2—FAST/SPS process flow diagram for the composite made by: (*a*) SPS, (*b*) R/SPS with description of changes in the anvil pressure, anvil movement, and temperature as a function of sintering time.

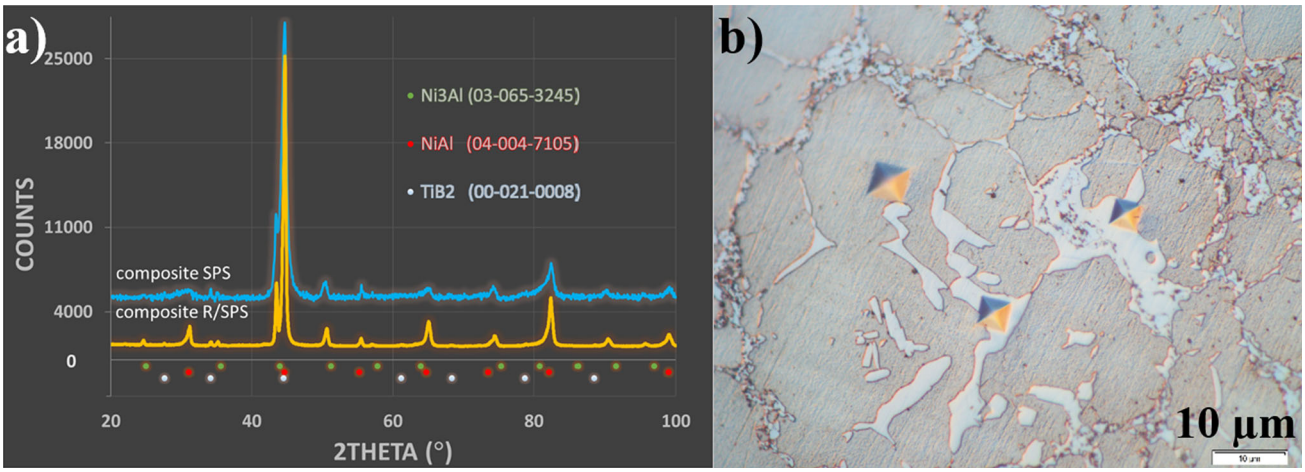

Fig. 3—(*a*) X-ray diffractogram of the manufactured sinters, (*b*) image of the SPS composite microstructure with indentations left by the HV0.05 microhardness tester—optical microscope.

were noticed during the test, not observed in earlier sintering processes of the SPS composite. The situation was similar when graphs were plotted during the manufacture of composite matrix (an alloy obtained from nickel and aluminum powders). In these graphs, in the vicinity of the temperature of 575 °C, a sudden "jump" of both temperature and piston stroke was observed, associated with the occurrence of rapid transformation caused by heat release—SHS. The sintering process was terminated at 1000 °C after the lapse of approximately 30 seconds from the instant of piston movement stabilization indicating almost full compaction of powder.

B. *Phase Analysis*

The X-ray analysis made for both types of produced sinters (Figure 3(a)) has confirmed the occurrence of NiAl, Ni_3Al, and TiB_2 phases. When the mixture of nickel-aluminum powders was heated, as a result of the SHS synthesis, a two-phase alloy composed of NiAl and Ni_3Al was formed. Neither the alloying process before and during the R/SPS and FAST/SPS sintering nor the introduction of TiB_2 ceramic particles in an amount of 3 wt pct to the mixture has resulted in the formation of an additional phase, especially from the NiAl system. No significant differences were observed in the diffraction patterns depending on the process of producing substrates for individual composites.

C. *Discussion of the Results Obtained for Selected Physical and Mechanical Properties*

Measurements show that, compared to the SPS composite, the density of the R/SPS composite is higher (ρ = 6.51 g/cm^3) and accounts for nearly 99.2 pct of the theoretical density (Table II). The Young's modulus and HV1 hardness are also slightly higher for the R/SPS composite (within the limits of statistical error). Hence, the conclusion follows that since for both these composites the obtained values are similar, differences in the composite manufacturing process are of no major importance.

Table II. Selected Properties of the Manufactured Composites

Composite	Density ρ_0 (g/cm^3)	ρ_0/ρ_{theo}. (Pct)	Young's Modulus E (GPa)	Vickers Hardness HV1	Poisson's Ratio v
SPS	6.46 ± 0.008	98.5	138 ± 4.0	504 ± 13.4	0.36
R/SPS	6.51 ± 0.013	99.2	142 ± 3.0	506 ± 37.9	0.35

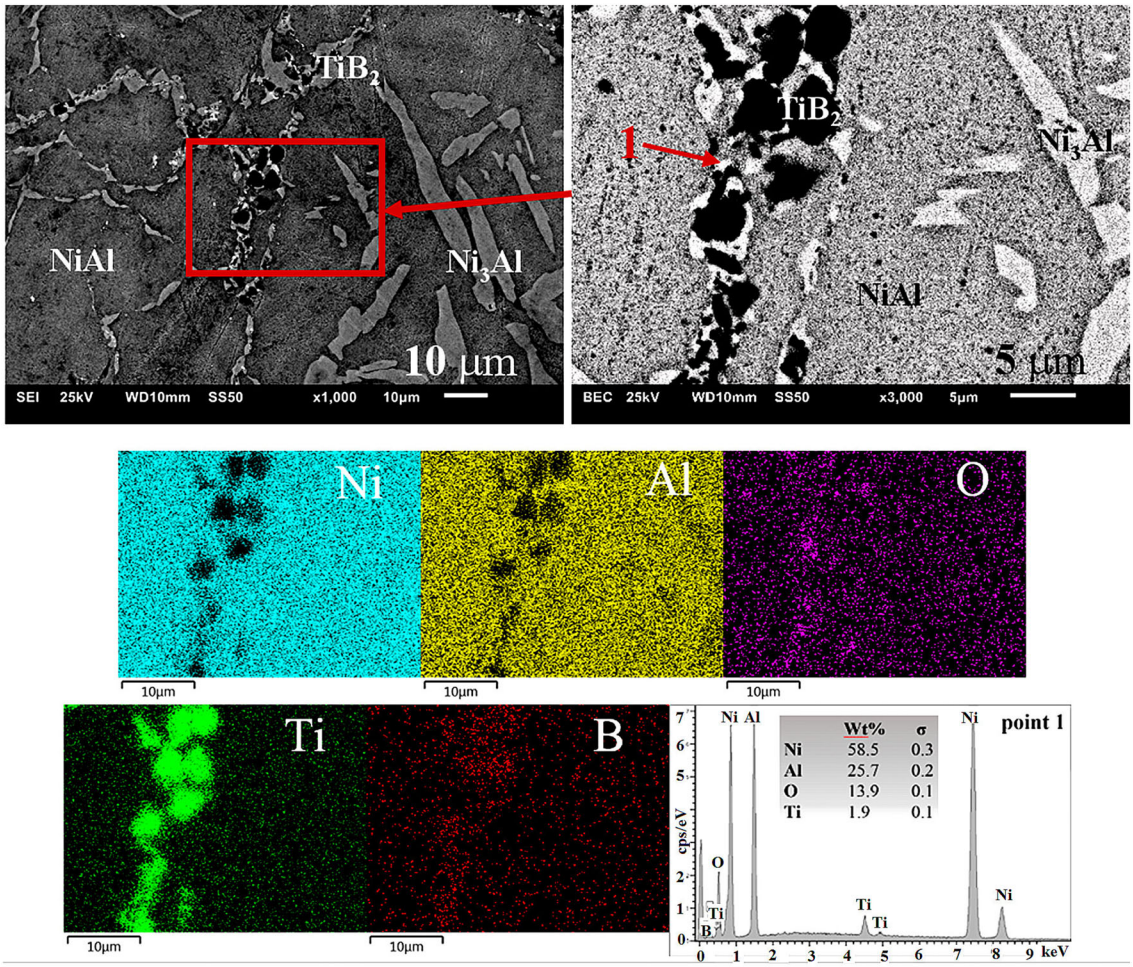

Fig. 4—Microstructure, map, and point EDS analysis of the SPS composite with distribution of oxides, TiB_2, and Ni_3Al on grain boundaries.

D. *Microstructure*

From microscopic observations it follows that all sinters produced are characterized by compact microstructure free from any visible microcracks or pores, often observed by other authors in similar studies.[4,30] The satisfactory results obtained in this study are mainly due to the application of the FAST/SPS sintering process.

Even first examinations of the microstructure reveal some differences between sinters made by SPS and R/SPS, but they may be due to the primary shape and size of grains and different history of the powder origin. In the SPS composite, grains composed of unevenly distributed internal areas forming a network or subgrains are present (Figures 3(b) and 4). Both EDS analysis and microhardness testing have identified these phases. The darker phase (with higher aluminum content) corresponds to the NiAl phase, while the lighter phase (with lower aluminum content) corresponds to the Ni_3Al phase. In both SPS and R/SPS composites, the phase identified as Ni_3Al and the particles of TiB_2 are evenly distributed around the grains. The size of the area occupied by the Ni_3Al phase is definitely larger in the R/SPS composite than in the SPS composite. Therefore, despite the similar size of Ni and Al grains, the R/SPS composite has a distinctly different structure than the SPS composite. This is also related to the previously described nickel powder structure. The observed microstructure seems to be composed of smaller grains than the size of the powder specified by the manufacturer

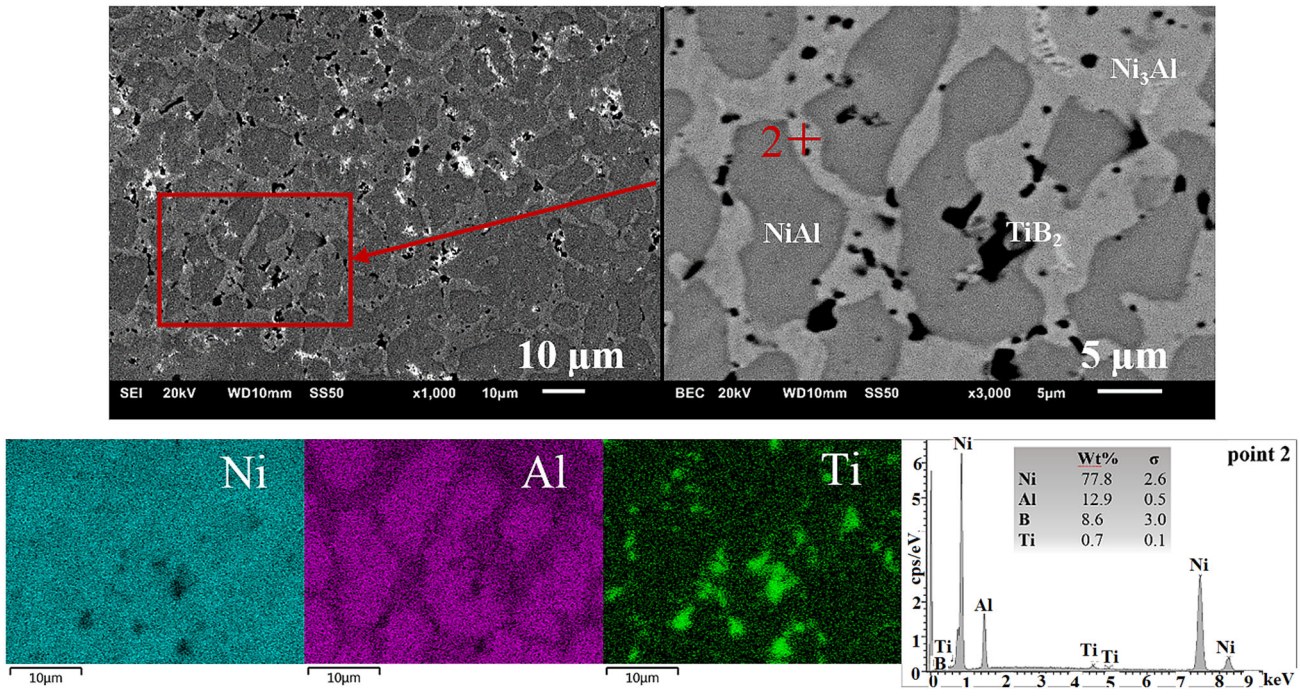

Fig. 5—Microstructure, map and point EDS analysis of the R/SPS composite with distribution of TiB_2 particles and Ni_3Al phase.

- smaller even than the powder used by Cui *et al.*, where the grain size was already very small (Ni powder < 38 μm and Al powder 38 to 50 μm particle size).[41]

Images of microstructures with maps showing uniform distribution of TiB_2 particles on grain boundaries are disclosed in Figures 4 and 5 for the SPS composite and R/SPS composite, respectively. Optimization of the manufacturing process will continue, including more uniform distributions due to improvements in the powder mixing process and mixture preparation.

From observations, EDS examinations of individual microstructure constituents, XRD analysis, and microhardness measurements, it follows that the content of the NiAl phase in the produced matrix is much higher than the content of the Ni_3Al phase, which was also confirmed by Cui *et al.* who in their studies determined the content of NiAl and Ni_3Al as 88.86 and 11.14 wt pct, respectively. The difference in relation to those studies may result from different Ni:Al quantitative ratios (2:1 and 1.75:1 respectively) and from the presence of TiB_2 particles introduced in an amount of 3 wt pct and distributed on grain boundaries. Studies of the images show that, despite some differences in the structure described earlier, the ratio of the NiAl phase to the Ni_3Al phase is similar for both sinters, *i.e.*, SPS and R/SPS.

E. *The Wear Characteristics*

The ball-on-disc friction test shows a higher coefficient of friction comprised in the range of 0.45 to 0.49 for the R/SPS composite against 0.4 to 0.45 for the SPS composite (Figure 6(a)), with the course of this dependence over time more stable for the R/SPS composite. In both cases, the coefficient of friction reaches its highest value in the last few minutes of the test, *i.e.*, in approximately 10,000th second. The linear intensity of wear is determined from the measured depth (height) of scar compared to the path of the tested material travel in contact with the ball at the point of abrasion. From the graph (changes in wear over time) it follows that the SPS composite characterized by a lower coefficient of friction wears out faster than the R/SPS composite. For both composites, the highest rate of wear has occurred in the first few minutes of the test (Figure 6(b)). For the R/SPS composite, the wear was lower in each subsequent second of the test and after 500 seconds it reached its minimum, then increased slightly, started decreasing again since 2000th second, to get finally stabilized and remain so till the end of the test. The situation was similar in the SPS composite, but in this case individual changes were much more pronounced (from the wear of 150 μm/km in 700th second to 50 μm/km in 1700th second of the test). The duration of the above-mentioned periods was longer, which means that the stabilization of wear this composite could achieve in approximately 6000th second, to reach at the end of the test the rate of wear similar to the R/SPS composite. The reason for these differences is to be searched in the occurrence of abrasive wear mechanism, additionally intensified by the effect of oxidation (especially in the case of SPS composite). Abrasive wear is characterized by the loss of material in the surface layer due to the detachment of particles by micro-cleavage, micro-scratching, or fissuring (Figure 7(a)). In the friction areas of cooperating elements there are loose (torn out) or fixed TiB_2 particles, or protruding fragments of the harder material - in this case the Ni_3Al phase (Figure 7(b)), which act as fixed sharp micro-edges. In

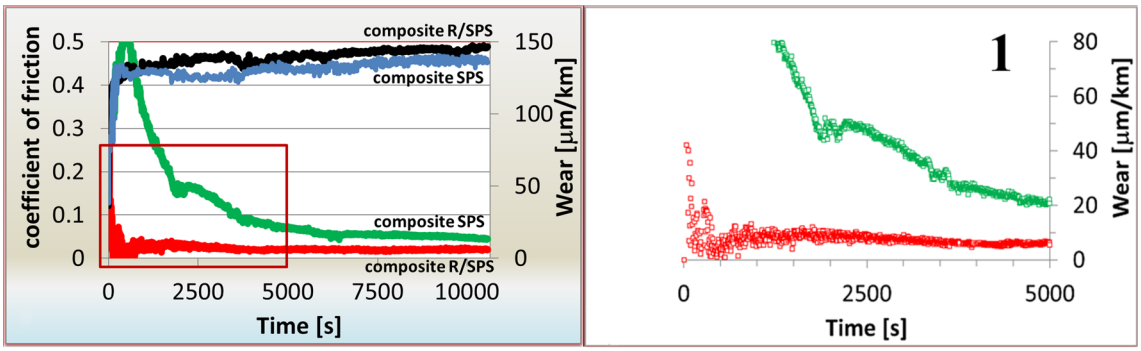

Fig. 6—Diagrams showing: (*a*) coefficient of friction and (*b*) linear intensity of wear as a function of the friction process time for SPS and R/SPS composites.

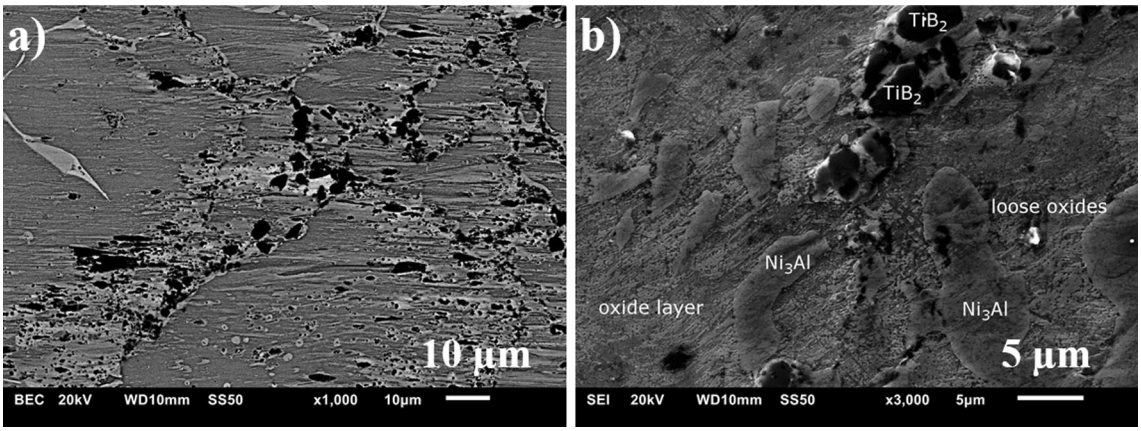

Fig. 7—Surface of the SPS composite after 2000 s of the friction process: (*a*) seizures and (*b*) the displaced TiB_2 particles, torn out surface components, and oxides.

the same way operate the oxidized wear products in the area of friction.

Oxidation wear can take another form when the intensity of oxide film formation is higher than the intensity of surface destruction through abrasion.[42,43] It has been shown that there are some basic differences in the coefficients of friction and wear intensity depending on the presence or absence of an oxide film.[44,45] The changes observed in the SPS composite can be attributed to the occurrence of wear as a result of oxidation and removal of the oxidized layers. According to Luong *et al.*,[46] the decrease in the coefficient of friction depends on the thickness of the oxide layer and its composition. A thicker oxide layer by increasing the lubrication at the interface can result in a lower coefficient of friction.[47] This explains the obtained test results and lower value of this coefficient observed for the SPS composite. Both friction and wear depend on the mechanical properties of the surfaces in contact, and in this particular case on the properties of oxides. Sliding speed and load affect heat generation in the actual contact area, which can change the nature (composition) of oxides, the growth rate of the oxide layer, and consequently the mechanism of wear. The formed tribolayer determines the tribological system and can protect or damage the sliding materials.[48–51] Conceição *et al.*[45] have indicated a reduction in the friction and wear occurring between two materials in the presence of an oxide film formed on the surface. In the case of the tested composites, the second mechanism of oxidation and the subsequent wear process were activated, resulting in the abrasion of hard oxidized layers from the friction surface, which next made furrows and abraded the parent material. Milan has demonstrated that oxides less hard can act as an additional factor reducing the wear intensity and the coefficient of friction, while harder, less adhering oxides can act as abrasives.[49] The SPS composite has the surface characterized by higher oxidation intensity (Figure 4(b)) than the R/SPS composite (Figure 5(b)). The highest rate of wear occurs in the first hour of the test, when fragments of the oxidized surface are removed by the action of abrasive materials and loose TiB_2 particles. The oxidized layer, thicker in SPS composites, wears away more rapidly and hence the obtained result. Fluctuations on the curve are caused by access to the next oxidized layer and the associated reduction in wear, also due to the surface strengthening effect. After wiping off the oxidized layers, the wear rate remains at a level equal with that observed in the R/SPS composite. Figures 4 and 8 show the images of

microstructure in the friction-unaffected and affected areas of the SPS composite. In the former case, oxides do not occur in the map analysis with the intensity so high as in the latter case. Hence, the conclusion follows that oxidation products are formed in the process of friction, also as a result of the temperature increase which makes them able to rebuild. Yet, at some point, these loose oxidation products are so numerous that the oxide layer is wiped off. Moreover, the occurrence of SHS in the R/SPS composite makes the TiB_2 particles more strongly embedded in the grain boundaries contrary to the SPS composite, where these particles are loosely deposited since they are introduced only after the reaction of synthesis has been completed. Therefore, they are pulled out more easily, have greater freedom of movement, and damage the cooperating surfaces by micro-scraping. Orrù has also confirmed the important role of SHS, especially in the production of sintered composites. Strong bonds are established between components, promoting diffusion during the next stage of SPS.[38] It was also observed that the migration of loose TiB_2 particles resulted in their accumulation in the form of aggregates (agglomerates).

"Loose particle"—torn out TiB_2 particles or oxidized components of the microstructure are moving and cause fissuring, micro-scraping, plastic deformation of layers lying on the front of the displaced oxidized particle, and sticking to other components of the microstructure

Examinations of the wear track left by the friction process showed the occurrence of the above-described mechanisms of the wear of composites. Figure 7 shows the microstructure of the SPS composite after 2000 seconds of the friction process with analysis and places of occurrence of the wear components, including oxides. Figure 8 shows the microstructure of the SPS composite after 10,000 seconds of the friction process, while Figure 9 shows the microstructure of the R/SPS composite after 10,000 seconds of the friction process. Cracks (furrows), torn out TiB_2 particles (Figure 9(a)), craters (black holes—Figure 10(b)), and seizures (containing both TiB_2 particles and unevenly displaced

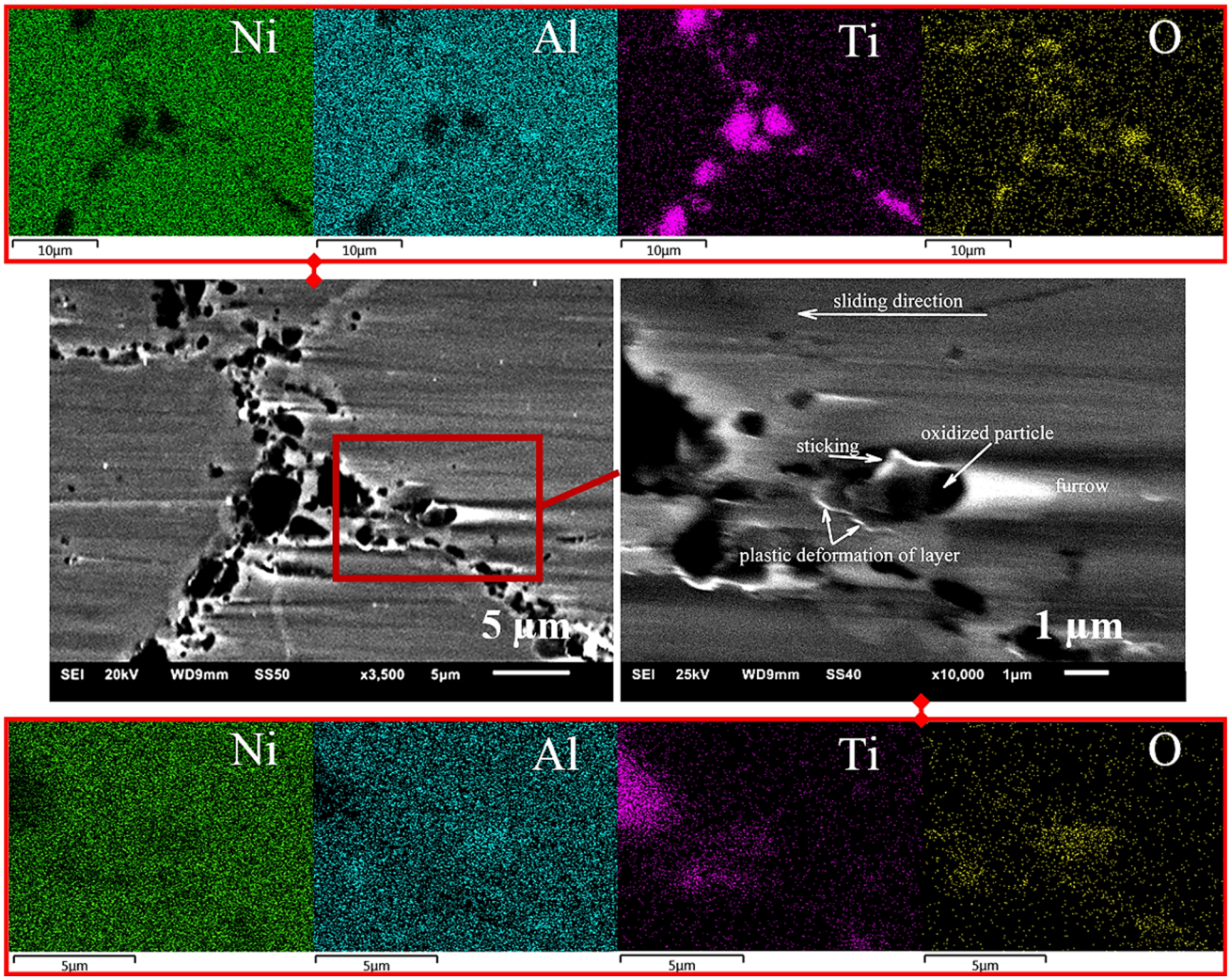

Fig.8—Surface of the SPS composite after 10,000 s of the friction process, scheme of destruction, "loose particle", maps of EDS analysis showing the displacement of oxidized microstructure elements.

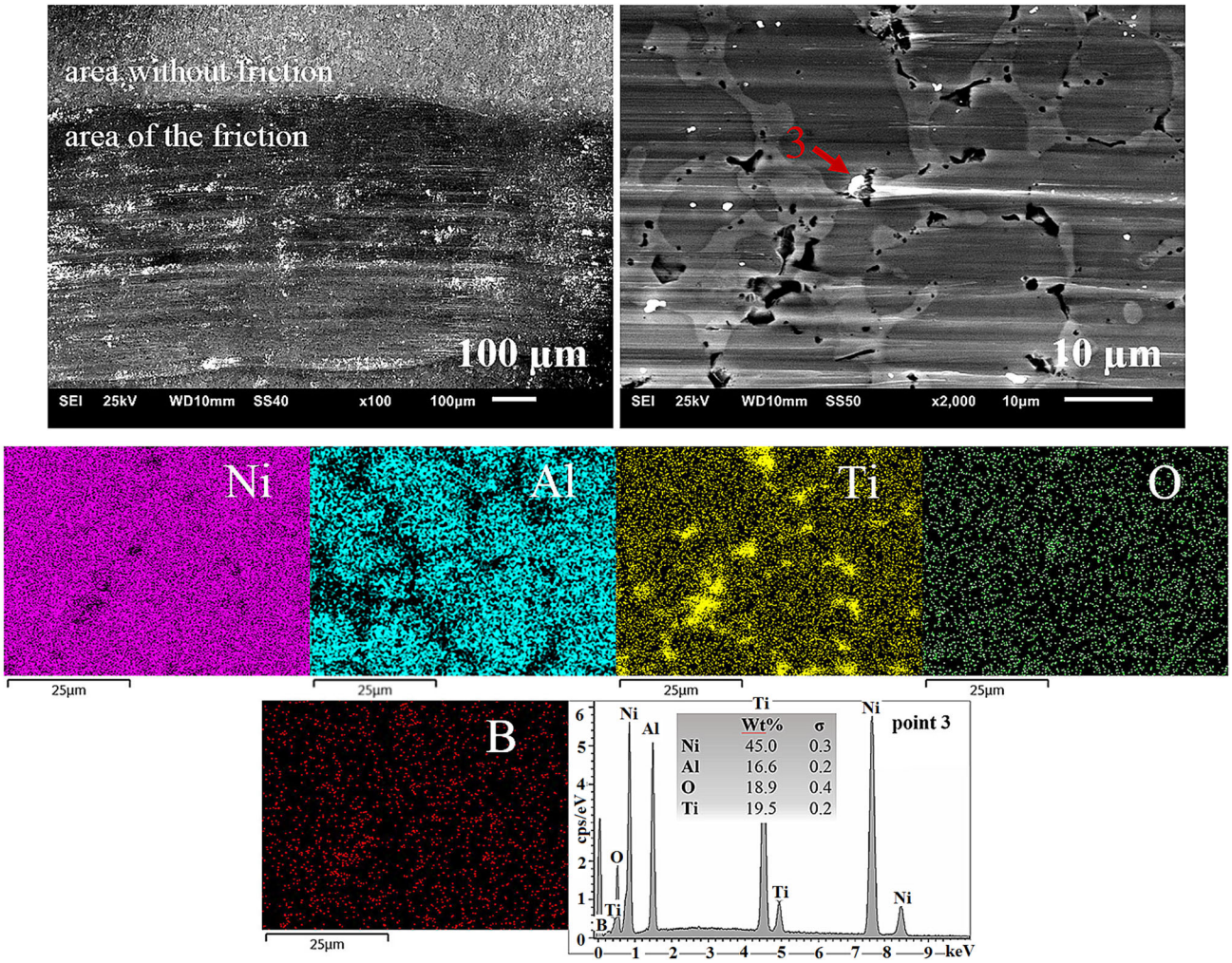

Fig. 9—Surface of the R/SPS composite after 10,000 s of the friction process showing torn out particles of TiB_2 and oxidized components of the microstructure (formed during friction process).

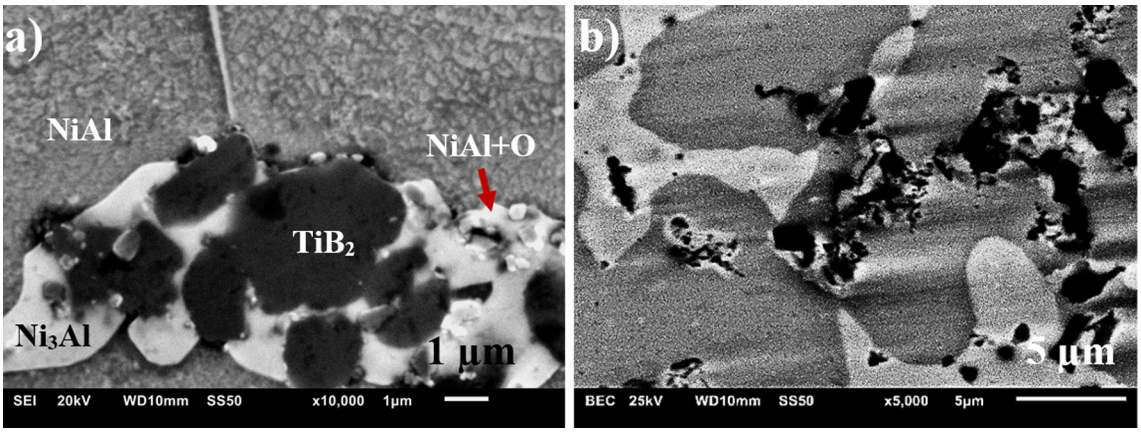

Fig. 10—(*a*) Seizure in the SPS composite after 2000 s of the friction process, (*b*) craters in the R/SPS composite after 10,000 s of the friction process.

matrix—Figures 7(a) and 10(a)) are visible. In the areas of seizures and craters, the presence of oxygen was identified. Additionally, plastic deformation of adjacent layers that surround moving particles and torn out oxidized 'loose' components of the microstructure were observed (Figures 8 and 9).

Table III. The Results of HV0.05 Microhardness Measurements of Selected Microstructure Constituents

	NiAl		Ni_3Al	
Composite	Microhardness HV0.05	Deviation (Pct)	Microhardness HV0.05	Deviation (Pct)
SPS	496	10.5	724	3.5
R/SPS	500	10.3	586	2.0

F. *Microhardness*

Compared to the tests conducted by Cui *et al*.,[41] the measured microhardness (Table III) of both NiAl phase (acting as a matrix) and Ni_3Al phase (precipitating on grain boundaries) is definitely higher, despite the use of apparently larger powder grains. The difference so great is probably due to the use of a different manufacturing process and the introduction of TiB_2 particles into the matrix (the effect of TiB_2 addition on the microhardness of NiAl has been documented, among others, in the tests conducted by Hou *et al*.[6]). Free sintering in a furnace at 650 °C for 0.5 hour could have an additional effect on the grain growth, although the description and photos provided by the authors do not confirm this statement. In the obtained composites, due to extreme heating and cooling rates, a relatively high concentration of defects has occurred, which could additionally influence the microhardness of individual microstructure constituents. The measured value of microhardness is about 500 HV0.05 for the phase corresponding to NiAl, and about 600 and 700 HV0.05 for the phase corresponding to Ni_3Al. The difference in the values obtained for the Ni_3Al phase probably results from a wide range of its occurrence on grain boundaries (R/SPS composite) and narrow range of occurrence in the grain area. It is also closely related to the effect of oxidation (SPS composite). For SPS composite, due to the narrow range of the occurrence of the Ni_3Al phase on grain boundaries, large differences were obtained in the values of HV0.05 microhardness. They are comprised in the range of 802 to 975 HV0.05 and are definitely higher than the values obtained for the interior part of grains and for the R/SPS composite. This is related to the oxidation of the Ni_3Al phase present in this composite on grain boundaries. The oxidized products are characterized by high microhardness and detached from the parent material aggravate the wear. The obtained results of wear confirm this statement. The distribution of oxides observed in the SPS composite prior to the friction process is shown in Figure 8.

Figure 3(b) shows a sample image of indentations left by the microhardness tester when individual microstructure constituents were examined in the SPS composite. Uneven and still not fully determined shape and distribution of individual phases, the size of these phases, and the large diversity in the microhardness values of individual phases—all these factors are responsible for the final profile of microhardness. Even when it seems that the measurement has ideally "hit" the selected phase, the results can be totally different. Therefore, these tests should be treated only as a guideline to demonstrate the occurrence of individual phases in the tested composite and roughly determine their distribution.

Careful analysis of the above results and comparison with Reference 37 lead to the conclusion that R/SPS sintering combined with the occurrence of exothermic reaction during compaction can give better results than the two-step sintering (fabrication of material by SHS reaction, milling to the form of powder and sintering). The above test results confirm this statement. By using the exothermic reaction during compaction, the material is manufactured at a lower temperature and in a much shorter time, while preserving similar properties in the end product. The microstructure is more compact, repeatable, homogeneous, and characterized by lower porosity, while TiB_2 particles, as demonstrated by tribological tests, have much better bond with the matrix and are more strongly embedded in the grain boundaries. The whole process is, however, more difficult to control. It is also more difficult to make the process operate in a uniform manner within the entire volume of the processed material, and hence probably result the differences in HV1 hardness observed on the cross-section of individual sintered compacts. It is therefore important to ensure proper preparation of the powder mixture and uniform distribution of the Ni, Al, and TiB_2 powders. To sum up, it can be said that to produce SPS composites, a mixture of nickel and aluminum was sintered, then the obtained product was ground and sieved, a composite mixture was prepared, and the whole was sintered by FAST/SPS. On the other hand, in the case of R/SPS composites, it was enough to perform the last two operations, namely mixing and sintering. So, even these short comments show us that the use of R/SPS saves time, electricity, and tools, also when individual substrates are made.

Further research will be carried out to determine the effect of the sintering method and SHS process on the properties of end product.

IV. CONCLUSIONS

As a result of the conducted research it was shown that the use of a reactive method in the production of NiAl composites by the SPS sintering process brings more benefits. Owing to the reduced temperature and time of the process, the use of R/SPS saves energy, which is reflected in the lower manufacturing cost and better environmental protection. Additionally, the occurrence of exothermic reaction produces compacts

with higher degree of sintering, higher density, lower porosity, and higher value of the Young's modulus. The density reaches 99 pct of the theoretical density, whereas for the (NiAl/Ni_3Al)/TiB_2 composite made by a two-step process in a longer time and at a higher temperature of sintering (with earlier exothermic reaction), the obtained density amounts to 98 pct of the theoretical value. Additionally, tribological tests carried out in a ball-on-disc system have been demonstrated that this composite, characterized by a lower coefficient of friction, undergoes faster wear than the R/SPS composite. The above changes can be explained by the occurrence of an abrasive wear mechanism that also occurs as a result of destruction with hard oxides. The occurrence of the reaction of synthesis in the R/SPS composite during powder compaction has made the TiB_2 particles more strongly embedded in the grain boundaries, in contrast to the SPS composite where the TiB_2 particles introduced after the process of synthesis were easily pulled out, could move in an unrestrained manner and damage the cooperating surfaces by micro-scraping.

Therefore the use of the reactive process seems to be particularly beneficial in the production of composites, since it contributes to the formation of more efficient bonding on the grain boundaries of powders, especially if the introduced grains include phases of so different quality as metal - ceramic systems. The use of this method not only saves energy needed for the product manufacture, but also reduces the risk of grain growth, which is particularly important in the fabrication of nanomaterials.

ACKNOWLEDGMENTS

This work was carried out with financial support through statutory funds of Pedagogical University in Cracow. Apparatus was co-financed by the European Regional Development Fund under the Infrastructure and Environment Programme: ''For the Development of the Infrastructure and Environment''.

OPEN ACCESS

REFERENCES

1. R. Darolia, W.S. Walston, M.V. Nathal: *Superalloys* (*8th Int. Symp.*), 1996, pp. 561–70.
2. R. Mitra, R.J.H. Wanhill: *Aerosp. Mater. and Mate. Technol., Indian Institute of Metals Series*, N. Prasad and R. Wanhill, eds., Springer, Singapore, 2017, pp. 229–45.
3. N.S. Stoloff, C.T. Liu, and S.C. Deevi: *Intermetallics*, 2000, vol. 8 (9–11), pp. 1313–20.
4. K. Morsi: *Mater. Sci. Eng. A*, 2001, vol. 299, pp. 1–15.
5. H.E. Camurlu and F. Maglia: *J. Alloys Compd.*, 2009, vol. 478, pp. 721–26.
6. S. Hou, Z. Liu, D. Liu, and Y. Ma: *Phys. Procedia*, 2012, vol. 32, pp. 71–77.
7. S. Talas: *Woodhead Publ. Ser. Compos. Sci. Eng.*, R. Mitra, eds., Elsevier, 2017, pp. 37–70.
8. S.K. Bhaumik, C. Divakar, L. Rangaraj, and A.K. Singh: Mater*Sci. Eng. A*, 1998, vol. 257 (2), pp. 341–48.
9. O. Umanskyi, O. Poliarus, M. Ukrainets, M. Antonov, and I. Hussainova: *Mater. Sci. (Medziagotyra)*, 2016, vol. 22 (1), pp. 49–53.
10. S.Z. Anvari, F. Karimzadeh, and M.H. Enayati: *J. Alloys Compd.*, 2009, vol. 477, pp. 178–81.
11. A.E. Karantzalis, A. Lekatou, and K. Tsirka: *Mater. Charact.*, 2012, vol. 69, pp. 97–107.
12. D.T. Jiang and J.T. Guo: Mater*Sci. Eng. A*, 1998, vol. 255 (1–2), pp. 154–61.
13. J.D. Whittenberger, R.K. Viswanadham, S.K. Mannan, and B. Sprissler: *J. Mater. Sci.*, 1990, vol. 25, pp. 35–44.
14. B. Wang and S.W. Lee: *Wear*, 2000, vol. 239 (1), pp. 83–90.
15. J.A. Hawk and D.E. Alman: *Wear*, 1999, vols. 225–229, pp. 544–56.
16. S. Zhu, Q. Bi, M. Niu, J. Yang, and W. Liu: *Wear*, 2012, vols. 274–275, pp. 423–34.
17. J.K. Sonber, T.S.R.Ch. Murthy, K. Sairam, A. Nagaraj, S. Majumdar, and V. Kain: *Int. J. Refract. Met. Hard Mater.*, 2018, vol. 70, pp. 56–65.
18. R.J. Arsenault: *Composites*, 1994, vol. 25 (7), pp. 540–48.
19. L. Wang, K. Xu, R.J. Arsenault: *Mat. Res. Soc. Symp. Proce. Intermet. Matrix Compos. III*, MRS, San Francisco, 1994, vol. 350, pp. 237–42.
20. P. Hyjek, I. Sulima, P. Malczewski, and L. Jaworska: *J. Achiev. Mater. Manuf. Eng.*, 2012, vol. 55 (2), pp. 700–05.
21. K. Martirosyan: *SHS 2013, Proc. of XII Int. Symp. on Self-Propag. High-Temp. Synth., South Padre Island*, 2013, pp. 11–46.
22. S.T. Aruna and A.S. Mukasyan: *Curr. Opin. Solid State Mater. Sci.*, 2008, vol. 12, pp. 44–50.
23. G. Xanthopoulou and G. Vekinis: *Adv. Environ. Res.*, 2001, vol. 5 (2), pp. 117–28.
24. N. Bertolino, M. Monagheddu, A. Tacca, P. Giuliani, C. Zanotti, F. Maglia, and U.A. Tamburini: *J. Mater. Res.*, 2003, vol. 18 (2), pp. 448–55.
25. N. Radishevskaya, O. Lepakova, N. Karakchieva, A. Nazarova, N. Afanasiev, A. Godymchuk, and A. Gusev: *Metals*, 2017, vol. 7, pp. 295–311.
26. K.C. Patil, S.T. Aruna, and T. Mimani: *Curr. Opin. Solid State Mater. Sci.*, 2002, vol. 6, pp. 507–12.
27. O. Yücel: SHS XIII Int. Symp. on self-propag. high temp. synth., abstract book, Antalya, 2015, pp. 72-95.
28. J.J. Moore and H.J. Feng: *Prog. Mater. Sci.*, 1995, vol. 39 (4–5), pp. 243–73.
29. X.Y. Jiao, X.H. Wang, and X.Q. Kang: *Mater. Manuf. Process.*, 2017, vol. 32 (5), pp. 489–94.
30. H.X. Dong, Y. Jiang, Y.H. He, M. Song, J. Zou, N.P. Xu, B.Y. Huang, C.T. Liu, and P.K. Liaw: *J. Alloys Compd.*, 2009, vol. 484, pp. 907–13.
31. A. Michalski, J. Jaroszewicz, M. Rosinski, and D. Siemiaszko: *Intermetallics*, 2006, vol. 14, pp. 603–06.
32. H.X. Dong, Y. Jiang, Y.H. He, J. Zou, N.P. Xu, B.Y. Huang, C.T. Liu, and P.K. Liaw: *Mater. Chem. Phys.*, 2010, vol. 122, pp. 417–23.
33. R. Orrù, G. Cao: *Concise Encycl. Self-Propagating High-Temperature Synth.*, 2017, pp. 349–51.
34. M. Suárez, A. Fernández, J.L. Menéndez, R. Torrecillas, H.U. Kessel, J. Hennicke, R. Kirchner, T. Kessel: *Sinter. Appl.*, InTech, 2013, pp. 319–42.
35. M. Tokita: *J. Soc. Powder Technol. Jpn.*, 1993, vol. 30(11), pp. 790–804.
36. R. Orrù, R. Licheri, A.M. Locci, A. Cincotti, and G. Cao: *Mater. Sci. Eng. R*, 2009, vol. 63, pp. 127–287.
37. A. Michalcová, D. Vojtech, T.F. Kubatík, P. Novák, P. Dvorák, P. Svobodová, and I. Marek: *Mater. Technol.*, 2016, vol. 50 (3), pp. 447–50.

38. R. Orrù and G. Cao: *Materials*, 2013, vol. 6 (5), pp. 1566–83.
39. P. Hyjek, I. Sulima, P. Pałka, L. Jaworska: *Met. 2016—25th Anniv. Int. Conf. Metall. Mater. Conf. Proc.*, 2016, pp. 1285–93.
40. P. Hyjek, I. Sulima, and L. Jaworska: *Arch. Metall. Mater.*, 2017, vol. 62 (3), pp. 1511–20.
41. H. Cui, N. Wei, L. Zeng, X. Wang, and H. Tang: *Trans. Nonferrous Met. Soc. China*, 2013, vol. 23, pp. 1639–45.
42. M. Hebda, A. Wachal: *Tribology* (in Polish), WNT, Warsaw 2010. http://www.tribologia.eu/ptt/try/tr.htm.
43. I. Hutchings and P. Shipway: *Tribology: Friction and Wear of Engineering Materials*, 2nd ed., Butterworth-Heinemann, London, 2017, pp. 165–236.
44. A. Mishra: *Int. J. Mech. Eng. Rob. Res.*, 2014, vol. 3 (3), pp. 598–602.
45. L. Conceição and A.S.C.M. D'Oliveira: *Surf. Coat. Technol.*, 2016, vol. 288, pp. 69–78.
46. L.H.S. Luong and T. Heijkoop: *Wear*, 1981, vol. 71 (1), pp. 93–102.
47. P.A. Munther and J.G. Lenard: *J. Mater. Process. Technol.*, 1999, vol. 88 (1–3), pp. 105–13.
48. G. Li, S.G. Qu, Y.X. Pan, X.Q. Li, and F.J. Sun: *J. Mater. Eng. Perform.*, 2017, vol. 26 (7), pp. 3489–99.
49. J.C.G. Milan, M.A. Carvalho, R.R. Xavier, S.D. Franco, and J.D.B. De Mello: *Wear*, 2005, vol. 259, pp. 412–23.
50. D. Kim and K. Kim: *Wear*, 2013, vol. 297 (1–2), pp. 722–30.
51. H. So, D.S. Yu, and C.Y. Chuang: *Wear*, 2002, vol. 253, pp. 1004–15.